A HIGHLY EFFICIENT CONDITIONAL MOMENT ALGORITHM FOR TRANSIENT FLOW IN RANDOM POROUS MEDIA

Ming Ye and Shlomo P. Neuman

neuman@hwr.arizona.edu

Department of Hydrology and Water Resources, University of Arizona, Tucson, Arizona, USA

Alberto Guadagnini

alberto.guadagnini@polimi.it

Dipartimento di Ingegneria Idraulica Ambientale e del Rilevamento, Politecnico di Milano, Milan, Italy

Daniel M. Tartakovsky

dmt@lanl.gov

Los Alamos National Laboratory, Los Alamos, New Mexico, USA

ABSTRACT

We present a highly efficient parallel computational algorithm for transient flow in random porous media of finite extent subject to uncertain forcing terms. The algorithm combines finite elements with numerical Laplace transform inversion to solve recursive approximations of otherwise exact nonlocal equations for the mean and variance-covariance of hydraulic head and flux. The random head and flux are nonstationary in space-time due to arbitrary forcing and conditioning on measured values of hydraulic conductivity at discrete points in space. Recursive approximation is carried to second order in log hydraulic conductivity conditional standard estimation error. The conditional moment solution compares well with "ground truth" Monte Carlo simulations of superimposed mean-uniform and convergent flows in a rectangular domain when log hydraulic conductivity exhibits large random fluctuations. The algorithm requires much less computer time than is needed for Monte Carlo statistics to stabilize, regardless of whether both solutions are computed sequentially or in parallel. The computational advantage of the parallel moment algorithm over parallel Monte Carlo simulations becomes more pronounced as grid size increases. Another computational advantage of the moment algorithm is that it allows analyzing a variety of flow scenarios by modifying forcing term statistics without recomputing Green's functions as long as the boundary configuration remains unaltered.

KEYWORDS: random media, porous media, stochastic equations, moment equations, nonlocality, finite elements, Laplace transform, perturbation, parallel computing.

1. INTRODUCTION

The subsurface environment consists of natural soils and rocks whose hydraulic properties are best described as spatially correlated random fields [1]. Subsurface fluid flow takes place under the action of driving mechanisms whose exact nature, magnitude, and space-time distribution are generally uncertain. Hence the equations that govern flow in geologic media are generally stochastic.

To characterize the statistics of spatially varying subsurface medium properties such as hydraulic conductivity, one typically infers them from measurements at discrete borehole locations using geostatistical estimation techniques [2]. The corresponding estimates honor, and are thus conditional on, the measured data. Using these estimates and corresponding estimation error statistics (typically their conditional variance and spatial autcovariance) as input should allow one, in principle, to solve the stochastic flow equations in terms of leading conditional moments of dependent variables such as hydraulic head and flux [3]. The most common way to accomplish this is to conduct conditional Monte Carlo simulations. This is done by generating numerous equally likely realizations of a correlated random hydraulic conductivity field on a grid that is fine enough to allow resolving high-frequency spatial fluctuations, while honoring available measurements; simulating flow due to each realization by computing numerically the corresponding space-time distributions of head and flux; and estimating their sample statistics (most commonly conditional mean, variance and covariance). The approach requires specifying the joint, multivariate probability distribution of hydraulic conductivity (as well as of forcing terms) at all grid points. It is computationally demanding and lacks well-established convergence criteria.

We focus on an alternative that allows computing the first two conditional moments of head and flux directly by solving a corresponding system of conditional moment equations. Our interest lies in the solution of transient stochastic flow problems of the kind previously considered by [4]. These authors developed exact integro-differential equations for the first two conditional moments of head and flux in a bounded, randomly heterogeneous domain. Their equations are nonlocal and non-Darcian in that the mean flux depends on mean head gradients at more than one point in space-time. The equations are exact in that they fully capture the first two conditional moments in only a few formal terms including domain and boundary integrals, which incorporate all relevant initial and boundary conditions. As a result of conditioning and the inclusion of arbitrary forcing terms, the statistics of both the input and the output variables are generally nonstationary in space-time. To render their exact formalism workable, the authors approximated their moment equations recursively through expansion in powers of σ_Y, the conditional standard deviation of (natural) log hydraulic conductivity $Y = \ln K$. Their recursive approximations are nominally limited either to mildly heterogeneous or to well-conditioned strongly heterogeneous media with $\sigma_Y \ll 1$.

In this paper we develop a highly accurate and efficient computational algorithm for the solution of nonlocal transient moment equations similar to those developed by [4]. After applying the Laplace transform to the governing stochastic flow equations, we derive exact nonlocal equations for the mean and variance-covariance of transformed head and flux, conditioned on measured values of *Y*. Approximating these conditional moment equations recursively to second order in σ_Y allows us to solve them by a finite element algorithm patterned after that developed for steady state flow by [5, 6]. We do so for superimposed mean-uniform and convergent flows in a two-dimensional domain. The solution is obtained using a highly

efficient parallel algorithm coupled with numerical inversion back into the time domain based on the method of [7]. The nonlocal solutions are compared with Monte Carlo simulations to assess their relative accuracies and computational efficiencies using single and multiple processors.

2. GOVERNING STOCHASTIC EQUATIONS

We consider transient flow in a domain Ω governed by Darcy's law

$$\mathbf{q}(\mathbf{x},t) = -K(\mathbf{x})\nabla h(\mathbf{x},t) \qquad \mathbf{x} \in \Omega \tag{1}$$

and the continuity equation

$$S_s(\mathbf{x})\frac{\partial h}{\partial t} = -\nabla \cdot \mathbf{q}(\mathbf{x},t) + f(\mathbf{x},t) \qquad \mathbf{x} \in \Omega \tag{2}$$

subject to initial and boundary conditions

$$h(\mathbf{x},0) = H_0(\mathbf{x}) \qquad \mathbf{x} \in \Omega \tag{3}$$

$$h(\mathbf{x},t) = H(\mathbf{x},t) \qquad \mathbf{x} \in \Gamma_D \tag{4}$$

$$-\mathbf{q}(\mathbf{x},t) \cdot \mathbf{n}(\mathbf{x}) = Q(\mathbf{x},t) \qquad \mathbf{x} \in \Gamma_N \tag{5}$$

where $\mathbf{q}$ is Darcy flux, $\mathbf{x}$ is a vector of space coordinates, t is time, K is scalar hydraulic conductivity forming a correlated random field, h is hydraulic head, S_s is a deterministic specific storage term, f is a random source term, $H_0(\mathbf{x})$ is random initial head, H is random head on Dirichlet boundaries Γ_D, Q is random flux into the flow domain across Neumann boundaries Γ_N, and $\mathbf{n}$ is a unit outward normal to the boundary $\Gamma = \Gamma_D \cup \Gamma_N$. The forcing terms f, H_0, H and Q are taken to be uncorrelated with each other or with K.

Taking the Laplace transform of the stochastic equations (1) – (5) yields the transformed flow equations

$$\bar{\mathbf{q}}(\mathbf{x},\lambda) = -K(\mathbf{x})\nabla \bar{h}(\mathbf{x},\lambda) \qquad \mathbf{x} \in \Omega \tag{6}$$

$$\nabla \cdot \bar{\mathbf{q}}(\mathbf{x},\lambda) + S_s(\mathbf{x})\lambda \bar{h}(\mathbf{x},\lambda) = \bar{f}(\mathbf{x},\lambda) + S_s(\mathbf{x})H_0(\mathbf{x}) \qquad \mathbf{x} \in \Omega \tag{7}$$

$$\bar{h}(\mathbf{x},\lambda) = \bar{H}(\mathbf{x},\lambda) \qquad \mathbf{x} \in \Gamma_D \tag{8}$$

$$-\bar{\mathbf{q}}(\mathbf{x},\lambda) \cdot \mathbf{n}(\mathbf{x}) = \bar{Q}(\mathbf{x},\lambda) \qquad \mathbf{x} \in \Gamma_N \tag{9}$$

where the overbar indicates Laplace transform.

Let $< K(\mathbf{x}) >_c$ be the ensemble mean of $K(\mathbf{x})$ conditioned on measurements at a set of discrete points in Ω. The random hydraulic conductivity $K(\mathbf{x})$ differs from its unbiased conditional estimate $< K(\mathbf{x}) >_c$ by a zero mean random estimation error $K'(\mathbf{x})$ such that

$$K(\mathbf{x}) =< K(\mathbf{x}) >_c + K'(\mathbf{x}) \qquad < K'(\mathbf{x}) >_c = 0 \tag{10}$$

Likewise we write

$$\bar{h}(\mathbf{x},\lambda) =< \bar{h}(\mathbf{x},\lambda) >_c + \bar{h}'(\mathbf{x},\lambda) \qquad < \bar{h}'(\mathbf{x},\lambda) >_c = 0 \tag{11}$$

$$\bar{\mathbf{q}}(\mathbf{x},\lambda) =< \bar{\mathbf{q}}(\mathbf{x},\lambda) >_c + \bar{\mathbf{q}}'(\mathbf{x},\lambda) \qquad < \bar{\mathbf{q}}'(\mathbf{x},\lambda) >_c = 0 \tag{12}$$

where $< \bar{h}(\mathbf{x},\lambda) >_c$ and $< \bar{\mathbf{q}}(\mathbf{x},\lambda) >_c$ constitute optimum unbiased predictors of head and flux conditioned on discrete measurements of $K(\mathbf{x})$, and $\bar{h}'(\mathbf{x},\lambda)$ and $\bar{\mathbf{q}}'(\mathbf{x},\lambda)$ are corresponding prediction errors.

A compact set of exact, nonlocal (integro-differential) equations governing the spatial distribution of $< \bar{h}(\mathbf{x},\lambda) >_c$, $< \bar{\mathbf{q}}(\mathbf{x},\lambda) >_c$ and the variance-covariance of $\bar{h}'(\mathbf{x},\lambda)$ and $\bar{\mathbf{q}}'(\mathbf{x},\lambda)$ is found in [8]; corresponding equations in space-time are given by [4].

3. CONDITIONAL RECURSIVE MOMENT EQUATIONS

The exact conditional moment equations in [8] are formally exact but contain unknown moments of a random Green's function. To render the exact moment equations workable we expand them to second order in σ_Y, the conditional standard deviation of (natural) log

conductivity $Y(\mathbf{x}) = \ln K(\mathbf{x})$ about its conditional mean, $< Y(\mathbf{x}) >_c$. The latter and the conditional variance-covariance of the zero-mean log conductivity fluctuations $Y'(\mathbf{x}) = Y(\mathbf{x}) - < Y(\mathbf{x}) >_c$ are inferred in practice from discrete measurements of conductivity using geostatistical methods [2]; we take them to be given. The perturbation yields recursive conditional first and second moment equations similar in principle to those originally developed in space-time by [4]. The recursive approximations are nominally limited either to mildly nonuniform log conductivity fields or to well-conditioned strongly nonuniform fields with $\sigma_Y \ll 1$.

Perturbation of the exact mean flow equation yields a system of zero-order (indicated by superscript 0 encased in parentheses) conditional mean head and flux equations

$$< \overline{\mathbf{q}}^{(0)}(\mathbf{x},\lambda) >_c = -K_G(\mathbf{x}) \nabla < \overline{h}^{(0)}(\mathbf{x},\lambda) >_c \qquad \mathbf{x} \in \Omega \tag{13}$$

$$\nabla \cdot < \overline{\mathbf{q}}^{(0)}(\mathbf{x},\lambda) >_c + S_s(\mathbf{x}) \lambda < \overline{h}^{(0)}(\mathbf{x},\lambda) >_c = < \overline{f}(\mathbf{x},\lambda) > + S_s(\mathbf{x}) < H_0(\mathbf{x}) > \qquad \mathbf{x} \in \Omega \tag{14}$$

$$< \overline{h}^{(0)}(\mathbf{x},\lambda) >_c = < \overline{H}(\mathbf{x},\lambda) > \qquad \mathbf{x} \in \Gamma_D \tag{15}$$

$$- < \overline{\mathbf{q}}^{(0)}(\mathbf{x},\lambda) >_c \cdot \mathbf{n}(\mathbf{x}) = < \overline{Q}(\mathbf{x},\lambda) > \qquad \mathbf{x} \in \Gamma_N \tag{16}$$

where $K_G(\mathbf{x}) = \exp < Y(\mathbf{x}) >_c$ is the conditional geometric mean of K and $< \overline{f} >$, $< H_0 >$, $< \overline{H} >$ and $< \overline{Q} >$ are ensemble mean forcing terms (assumed here to be unconditional and given). Second order corrections of head and flux are governed by

$$< \overline{\mathbf{q}}^{(2)}(\mathbf{x},\lambda) >_c = -K_G(\mathbf{x}) [\nabla < \overline{h}^{(2)}(\mathbf{x},\lambda) >_c + \frac{\sigma_Y^2(\mathbf{x})}{2} \nabla < \overline{h}^{(0)}(\mathbf{x},\lambda) >_c] + \overline{\mathbf{r}}_c^{(2)}(\mathbf{x},\lambda) \qquad \mathbf{x} \in \Omega \tag{17}$$

$$\nabla \cdot < \overline{\mathbf{q}}^{(2)}(\mathbf{x},\lambda) >_c + S_s(\mathbf{x}) \lambda < \overline{h}^{(2)}(\mathbf{x},\lambda) >_c = 0 \qquad \mathbf{x} \in \Omega \tag{18}$$

$$< \overline{h}^{(2)}(\mathbf{x},\lambda) >_c = 0 \qquad \mathbf{x} \in \Gamma_D \tag{19}$$

$$- < \overline{\mathbf{q}}^{(2)}(\mathbf{x},\lambda) >_c \cdot \mathbf{n}(\mathbf{x}) = 0 \qquad \mathbf{x} \in \Gamma_N \tag{20}$$

where $\sigma_Y^2(\mathbf{x}) =< Y'^2(\mathbf{x}) >_c$ is the conditional variance of $Y(\mathbf{x})$;

$$\begin{aligned}&\bar{\mathbf{r}}_c^{(2)}(\mathbf{x},\lambda) = \\ &\int_\Omega K_G(\mathbf{x})K_G(\mathbf{y}) < Y'(\mathbf{x})Y'(\mathbf{y}) >_c \nabla_{\mathbf{x}}\nabla_{\mathbf{y}}^T < \bar{G}^{(0)}(\mathbf{y},\mathbf{x},\lambda) >_c \nabla_{\mathbf{y}} < \bar{h}^{(0)}(\mathbf{y},\lambda) >_c d\mathbf{y}\end{aligned} \tag{21}$$

is a second-order approximation of the "residual flux" $\bar{\mathbf{r}}_c(\mathbf{x},\lambda) = - < K'(\mathbf{x})\nabla\bar{h}'(\mathbf{x},\lambda) >_c$; $< Y'(\mathbf{x})Y'(\mathbf{y}) >_c$ is the (given) conditional covariance of Y between points $\mathbf{x}$ and $\mathbf{y}$; and $< \bar{G}^{(0)}(\mathbf{y},\mathbf{x},\lambda) >_c$ is the zero-order approximation of a random Green's function associated with (6) – (9), obtained upon solving (13) – (16) subject to homogeneous boundary conditions and a Dirac delta source. We approximate mean head and flux by their two leading-order terms,

$$\begin{aligned}&< \bar{h}(\mathbf{x},\lambda) >_c \approx < \bar{h}^{(0)}(\mathbf{x},\lambda) >_c + < \bar{h}^{(2)}(\mathbf{x},\lambda) >_c \\ &< \bar{\mathbf{q}}(\mathbf{x},\lambda) >_c \approx < \bar{\mathbf{q}}^{(0)}(\mathbf{x},\lambda) >_c + < \bar{\mathbf{q}}^{(2)}(\mathbf{x},\lambda) >_c\end{aligned} \tag{22}$$

The conditional head variance $C_{hc}(\mathbf{x},\mathbf{x},t,t) =< h'(\mathbf{x},t)h'(\mathbf{x},t) >_c$ at $(\mathbf{x},t)$ is the inverse Laplace transform of the covariance $\bar{C}_{hc}(\mathbf{x},\mathbf{x},\lambda,t) =< \bar{h}'(\mathbf{x},\lambda)h'(\mathbf{x},t) >_c$ between transformed and original head. The latter is given to leading order of approximation by

$$\begin{aligned}&\bar{C}_{hc}(\mathbf{x},\mathbf{x},\lambda,t) \approx \bar{C}_{hc}^{(2)}(\mathbf{x},\mathbf{x},\lambda,t) = \\ &-\int_\Omega u_c^{(2)}(\mathbf{y},\mathbf{x},t)\nabla_{\mathbf{y}} < \bar{h}^{(0)}(\mathbf{y},\lambda) >_c \cdot\nabla_{\mathbf{y}} < \bar{G}^{(0)}(\mathbf{y},\mathbf{x},\lambda) >_c d\mathbf{y} \\ &+\int_0^t\int_\Omega\int_\Omega \bar{C}_f(\mathbf{y},\mathbf{z},\lambda,\tau) < G^{(0)}(\mathbf{z},\mathbf{x},t-\tau) >_c < \bar{G}^{(0)}(\mathbf{y},\mathbf{x},\lambda) >_c d\mathbf{z}d\mathbf{y}d\tau \\ &+\int_\Omega\int_\Omega S_s(\mathbf{y})S_s(\mathbf{z})C_{H_0}(\mathbf{y},\mathbf{z}) < G^{(0)}(\mathbf{z},\mathbf{x},t) >_c < \bar{G}^{(0)}(\mathbf{y},\mathbf{x},\lambda) >_c d\mathbf{z}d\mathbf{y} \\ &+\int_0^t\int_{\Gamma_D}\int_{\Gamma_D} \bar{C}_H(\mathbf{y},\mathbf{z},\lambda,\tau)K_G(\mathbf{z})\nabla_{\mathbf{z}} < G^{(0)}(\mathbf{z},\mathbf{x},t-\tau) >_c \cdot\mathbf{n}(\mathbf{z}) \\ &\qquad\qquad K_G(\mathbf{y})\nabla_{\mathbf{y}} < \bar{G}^{(0)}(\mathbf{y},\mathbf{x},\lambda) >_c \cdot\mathbf{n}(\mathbf{y})d\mathbf{z}d\mathbf{y}d\tau \\ &+\int_0^t\int_{\Gamma_N}\int_{\Gamma_N} \bar{C}_Q(\mathbf{y},\mathbf{z},\lambda,\tau) < G^{(0)}(\mathbf{z},\mathbf{x},t-\tau) >_c < \bar{G}^{(0)}(\mathbf{y},\mathbf{x},\lambda) >_c d\mathbf{z}d\mathbf{y}d\tau\end{aligned} \tag{23}$$

where $u_c^{(2)}(\mathbf{y},\mathbf{x},t)$ is the inverse Laplace transform of $\overline{u}_c^{(2)}(\mathbf{y},\mathbf{x},\lambda)$, a second-order approximation of the cross-covariance $\overline{u}_c(\mathbf{y},\mathbf{x},\lambda) =< K'(\mathbf{y})\overline{h}'(\mathbf{x},\lambda) >_c$ between hydraulic head and conductivity, given explicitly by

$$\overline{u}_c^{(2)}(\mathbf{y},\mathbf{x},\lambda) = -K_G(\mathbf{y})\int_\Omega K_G(\mathbf{z}) < Y'(\mathbf{z})Y'(\mathbf{y}) >_c \nabla_{\mathbf{z}}^T < \overline{h}^{(0)}(\mathbf{z},\lambda) >_c \nabla_{\mathbf{z}} < \overline{G}^{(0)}(\mathbf{z},\mathbf{x},\lambda) >_c d\mathbf{z} \qquad (24)$$

and C_{H_0}, $\overline{C}_f$, $\overline{C}_H$ and $\overline{C}_Q$ are transformed covariances of the forcing terms (assumed to be known),

$$\begin{aligned} C_{H_0}(\mathbf{x},\mathbf{z}) &=< H_0'(\mathbf{x})H_0'(\mathbf{z}) > \\ \overline{C}_f(\mathbf{x},\mathbf{z},\lambda,\tau) &=< \overline{f}'(\mathbf{x},\lambda)f'(\mathbf{z},\tau) > \\ \overline{C}_H(\mathbf{x},\mathbf{z},\lambda,\tau) &=< \overline{H}'(\mathbf{x},\lambda)H'(\mathbf{z},\tau) > \\ \overline{C}_Q(\mathbf{x},\mathbf{z},\lambda,\tau) &=< \overline{Q}'(\mathbf{x},\lambda)Q'(\mathbf{z},\tau) > \end{aligned} \qquad (25)$$

For consistency, we assume that all random fluctuations in forcing terms are of order σ_Y. If driving forces are deterministic, (25) vanishes and (23) reduces to

$$\overline{C}_{hc}^{(2)}(\mathbf{x},\mathbf{x},\lambda,t) = -\int_\Omega u_c^{(2)}(\mathbf{y},\mathbf{x},t)\nabla_{\mathbf{y}} < \overline{h}^{(0)}(\mathbf{y},\lambda) >_c \cdot\nabla_{\mathbf{y}} < \overline{G}^{(0)}(\mathbf{y},\mathbf{x},\lambda) >_c d\mathbf{y} \qquad (26)$$

Corresponding approximations can be derived for cross-covariances between Laplace transformed head or flux and the original head or flux at any two points in space-time [8].

5. COMPUTATIONAL ALGORITHM

We solve the above recursive moment equations by the Galerkin method on a rectangular grid of square elements using bilinear Lagrange interpolation and weight functions φ. In particular, we write

$$\overline{p}(\mathbf{x},\lambda) \approx \sum_{m=1}^{N} \overline{p}_m(\lambda)\varphi_m(\mathbf{x}) \qquad (27)$$

where N is the number of nodes; $\overline{p}_m$ is a transformed dependent variable, such as $<\overline{h}^{(0)}>_c$, $<\overline{h}^{(2)}>_c$ or $\overline{C}_{hc}^{(2)}$, at node m; and $\varphi_m(\mathbf{x})$ is a bilinear Lagrange interpolation function satisfying $\varphi_m(\mathbf{x}_n)=\delta_{mn}$ where δ_{mn} is the Kronecker delta. Substituting (27) into the above recursive moment equations yields a system of finite element equations as shown below. In line with the inverse Laplace transform algorithm of [9], we discretize the transform parameter λ as

$$\lambda_k = \lambda_0 + ik\pi / T \qquad k = 0,1,2,...,2K+1 \tag{28}$$

where $\lambda_0 = -\ln(E)/(2T)$, E is a dimensionless discretization error (which we set equal to $E=10^{-6}$), $T=0.8t_{\max}$ and $t_{\max}$ is the simulation period (we set $K=23$). We solve the finite element equations $2(K+1)$ times for $\overline{h}_{jk}$, j = 1, 2, … N, once for each λ_k. As these solutions are mutually independent, we solve them in parallel on multiple processors. To compute the inverse Laplace transform of head at node j and time $t\in(0,t_{\max})$, we employ the quotient difference algorithm of [7],

$$h_j(t) = \frac{1}{T}\exp(\lambda_0 t)[\frac{1}{2}\overline{h}_{j0} + \sum_{k=1}^{2K+1}\mathrm{Re}\{\overline{h}_{jk}\exp(ik\pi t/T)\}] \tag{29}$$

Galerkin finite element equations corresponding to the zero-order mean flow equations (13) – (16) are standard and thus not shown. Galerkin orthogonalization of (17) – (20) yields the finite element equations (Appendix A)

$$\sum_{m=1}^{N}[A_{nm}+\lambda D_{nm}]\overline{h}_m^{(2)}(\lambda)+\sum_{m=1}^{N}B_{nm}\overline{h}_m^{(0)}(\lambda)=R_n+P_n \qquad n=1,2...N \tag{30}$$

where $\overline{h}_m^{(2)}(\lambda)$ is second-order conditional mean head correction at node m and the coefficients are computed according to

$$A_{nm}=\int_\Omega K_G(\mathbf{x})\nabla\varphi_n(\mathbf{x})\cdot\nabla\varphi_m(\mathbf{x})d\mathbf{x} \tag{31}$$

$$B_{nm} = \int_{\Omega} K_G(\mathbf{x}) \frac{\sigma_Y^2(\mathbf{x})}{2} \nabla \varphi_n(\mathbf{x}) \cdot \nabla \varphi_m(\mathbf{x}) d\mathbf{x} \tag{32}$$

$$D_{nm} = \int_{\Omega} S_s(\mathbf{x}) \varphi_n(\mathbf{x}) \varphi_m(\mathbf{x}) d\mathbf{x} \tag{33}$$

$$R_n = \int_{\Omega} \overline{\mathbf{r}}_c^{(2)}(\mathbf{x}, \lambda) \cdot \nabla \varphi_n(\mathbf{x}) d\mathbf{x} \tag{34}$$

$$P_n = -\int_{\Gamma_D} \frac{\sigma_Y^2(\mathbf{x})}{2} < \bar{Q}(\mathbf{x}, \lambda) > \varphi_n(\mathbf{x}) d\mathbf{x} - \int_{\Gamma_D} \overline{\mathbf{r}}_c^{(2)}(\mathbf{x}, \lambda) \cdot \mathbf{n}(\mathbf{x}) \varphi_n(\mathbf{x}) d\mathbf{x} \tag{35}$$

The matrices $\mathbf{A}$, $\mathbf{D}$ and $\mathbf{B}$ (with terms A_{nm}, D_{nm} and B_{nm}, respectively) are real-valued, sparse and symmetric. The second-order residual flux term $\overline{\mathbf{r}}_c^{(2)}(\mathbf{x}, \lambda)$ is computed via (Appendix B)

$$\overline{\mathbf{r}}_c^{(2)}(\mathbf{x}^e, \lambda) = K_G(\mathbf{x}^e) \sum_{i=1}^{N_x} \nabla_{\mathbf{x}} \varphi_i(\mathbf{x}) \Big|_{(\mathbf{x}=\mathbf{x}^e)} \sum_{e'=1}^{M_y} K_G(\mathbf{y}^{e'}) < Y'(\mathbf{x}^e) Y'(\mathbf{y}^{e'}) >_c \sum_{j=1}^{N_y} \sum_{k=1}^{N_y} \overline{G}_{ij}^{(0)ee'}(\lambda) \overline{h}_k^{(0)e'}(\lambda) \Delta_{jk}^{e'e'} \tag{36}$$

where N_x and N_y ($N_x = N_y = 4$) are the number of nodes in elements e and e' within the $\mathbf{x}$- and $\mathbf{y}$-planes, respectively; M_y is the number of elements in the y- plane; $\overline{G}_{ij}^{(0)ee'}$ is the zero-order mean Green's function at node i of element e in the $\mathbf{x}$-plane due to a unit source at node j of element e' in the $\mathbf{y}$-plane; $\overline{h}_k^{(0)e'}(\lambda)$ is $\overline{h}^{(0)}(\mathbf{y}, \lambda)$ at node k of element e' in the $\mathbf{y}$-plane; and

$$\Delta_{ij}^{e'e'} = \int_{e'} \nabla_{\mathbf{y}} \varphi_j^{e'}(\mathbf{y}) \cdot \nabla_{\mathbf{y}} \varphi_k^{e'}(\mathbf{y}) d\mathbf{y} \tag{37}$$

Treating log hydraulic conductivity as a constant in each element, the covariance $< Y'(\mathbf{x}) Y'(\mathbf{y}) >_c$ between any points $\mathbf{x}$ in element e and $\mathbf{y}$ in element e' is approximated by $< Y'(\mathbf{x}^e) Y'(\mathbf{y}^{e'}) >_c$, where $\mathbf{x}^e$ is the centroid of element e and $\mathbf{y}^{e'}$ is the centroid of element e'. Substituting (36) into (34) yields the finite element approximation

$$R_n = \sum_{e=1}^{M_x} K_G(\mathbf{x}^e) \sum_{i=1}^{N_x} \Theta_{ni}^{ee} \sum_{e'=1}^{M_y} K_G(\mathbf{y}^{e'}) < Y'(\mathbf{x}^e) Y'(\mathbf{y}^{e'}) >_c \sum_{j=1}^{N_y} \sum_{k=1}^{N_y} \overline{G}_{ij}^{(0)ee'}(\lambda) \overline{h}_k^{(0)e'}(\lambda) \Delta_{jk}^{e'e'} \tag{38}$$

where

$$\Theta_{ni}^{ee} = \int_e \nabla_{\mathbf{x}} \varphi_n^e(\mathbf{x}) \cdot \nabla_{\mathbf{x}} \varphi_i^e(\mathbf{x}) \, d\mathbf{x} \tag{39}$$

The finite element approximation of transformed head variance (25) is (Appendix B)

$$\overline{C}_{hc}^{(2)}(\mathbf{x}, \mathbf{x}, \lambda, t) = -\sum_{e'=1}^{M_y} u_{c;j_y}^{(2)e'}(\mathbf{x}, t) \sum_{i=1}^{N_y} \overline{G}_i^{(0)e'}(\mathbf{x}, \lambda) \sum_{j=1}^{N_y} \overline{h}_j^{(0)e'}(\lambda) \Delta_{ij}^{e'e'} \tag{40}$$

where $\overline{G}_i^{(0)e'}(\mathbf{x}, \lambda)$ is zero-order mean Green's function at node i within element e' in the **y**-plane due to a source of unit strength at node $\mathbf{x}$ within element e in the **x**-plane; $\overline{h}_j^{(0)e'}(\lambda)$ is zero-order conditional mean head at node j in the **y**-plane; $\Delta_{ij}^{e'e'}$ is given by (37); and $u_{c;j_y}^{(2)e'}(\mathbf{x}, t)$ is the inverse transform of $\overline{u}_{c;j_y}^{(2)e'}(\mathbf{x}, \lambda)$ corresponding to hydraulic conductivity at point $\mathbf{x}$ and transformed head at node j_y in the **y**-plane, given by

$$\overline{u}_{c;j_y}^{(2)e'}(\mathbf{x}, \lambda) = -K_G(\mathbf{x}^e) \sum_{e''=1}^{M_z} K_G(\mathbf{z}^{e''}) < Y'(\mathbf{x}^e) Y'(\mathbf{z}^{e''}) >_c \sum_{i_z=1}^{N_z} \sum_{j_z=1}^{N_z} \overline{G}_{i_z j_y}^{(0)e''}(\lambda) \overline{h}_{j_z}^{(0)e''}(\lambda) \Xi_{i_z j_z}^{e''e''} \tag{41}$$

Here M_z is the number of elements in the **z**-plane; $N_z = 4$ is the number of nodes in element e'' within the $\mathbf{z}$-plane; $\overline{h}_{j_z}^{(0)e''}(\lambda)$ is $\overline{h}_c^{(0)}(\mathbf{z}, \lambda)$ at node j_z in element e'' within the **z**-plane; $\overline{G}_{i_z j_y}^{(0)e''}$ is zero-order mean Green's function at node i_z in element e within the **z**-plane due to a source of unit strength at node j_y within element e'' in the **y**-plane; and

$$\Xi_{i_z j_z}^{e''e''} = \int_{e''} \nabla_z \varphi_{i_z}^{e''}(\mathbf{z}) \cdot \nabla_z \varphi_{j_z}^{e''}(\mathbf{z}) d\mathbf{z} \tag{42}$$

Corresponding finite element approximations can be derived for cross-covariances between Laplace transformed head or flux and the original head or flux at any two points [8]. All

of these moments are evaluated in parallel on multiple processors for discrete values of λ and inverted numerically back into the time domain using the aforementioned algorithm.

6. PARALLEL IMPLEMENTATION

Our moment algorithm was implemented on a SGI Origin 2000 supercomputer using Message Passing Interface (MPI) [10], which has the advantage of being portable across a variety of computing platforms. The platform included a distributed memory MIMD system with 88 processors at send/receive latency of 8 μsec and peak bandwidth of 150 $Mbytes/\sec$. SPMD (Single Program Multiple Data) programming was used to allow running the same code on each processor. We first computed $2(K+1)$ discrete Laplace transform parameters λ_k on a processor of rank zero and then distributed the task of solving the corresponding finite element equations to p processors using the collective communication function MPI_SCATTER. If $\mathrm{mod}(2(K+1), p) = 0$, then each processor contains $2(K+1)/p$ discretized Laplace parameters. Otherwise, a processor of rank $p-1$ was assigned $\mathrm{mod}(2(K+1), p)$ discretized Laplace parameters. To avoid facing a load-balancing problem between processors, we solved the finite element equations for each discrete value of λ_k using a direct (IMSL subroutine DLSLZG [11]) rather than an iterative solver [e.g., 12].

Although the inverse Laplace transform equation (35) could be implemented in parallel [e.g., 13], we found this unnecessary due to the relative speed of the corresponding sequential code.

Monte Carlo simulations were implemented using the same finite element and Laplace inversion schemes as those used to solve the zero-order moment equations. As realizations of Monte Carlo simulation are mutually independent, they were distributed among p processors using MPI_SCATTER.

7. COMPUTATIONAL EXAMPLE

To illustrate our approach we consider superimposed mean uniform and convergent flows in a two-dimensional rectangular domain with $M = 800$ square elements (20 rows and 40 columns) of uniform size $\Delta x_1 = \Delta x_2 = 0.2$ measured in arbitrary consistent length units (Figure 1). The length of the domain is $L_1 = 40 \times 0.2 = 8$ and its width is $L_2 = 20 \times 0.2 = 4$. A uniform deterministic head $H_L = 8$ (in similar length units) is prescribed on the left boundary ($x_1 = 0$) and a constant head $H_R = 4$ on the right boundary ($x_1 = 8$). The bottom ($x_2 = 0$) and top ($x_2 = 4$) boundaries are impermeable. Constant deterministic initial head $H_0 = 4$ is assigned to all but the prescribed head boundary nodes of the grid. A point sink (pumping well) of deterministic strength Q_p (in arbitrary consistent units of length per time) is placed at the center node of the domain ($x_1 = 4, x_2 = 2$). Transient flow is simulated over a period $t_{sim} = 20$ of similar time units. Solutions of the finite element equations are obtained at discrete time steps $t = 1, 2, ...20$ spaced uniformly at unit intervals $\Delta t = 1$. We employ the same computational grid and time steps for all moment and Monte Carlo solutions to render them directly comparable.

The log conductivity field is taken to be stationary and isotropic with exponential covariance function $C(r) = \sigma_Y^2 \exp(-r/l)$, where r is separation distance (lag) between two points in the domain and l is the (integral) correlation scale. For purposes of Monte Carlo simulation we assume that Y is multivariate Gaussian (no such distributional assumption is required for the moment solution). Random Y fields are generated using the sequential Gaussian simulation code SGSIM [14]. Each element is assigned a constant conductivity corresponding to the value generated at its center. We first generate one unconditional realizations of Y with mean $< Y > = 0$, variance $\sigma_Y^2 = 1$ and correlation scale $l = 1$. We then "measure" Y (without

error) at 12 evenly-distributed conditioning points shown by dark squares in Figure 1 and generate 2000 corresponding conditional realizations of Y.

The first two sample moments of these realizations are used as input into our conditional moment algorithm and Monte Carlo simulation to render the comparison of their solutions meaningful. Figure 2 depicts an image of the conditional sample variance S_Y^2 of conditional log conductivity and two corresponding profiles. Conditioning clearly reduces the sample variance below its uniform unconditional value of 1. At conditioning points (marked by open circles) the sample variance is zero.

Monte Carlo simulations consist of solving equations (6) – (9) for each realization and computing the first two sample moments of the results. Convergence of the MC simulation process is diagnosed by examining the way in which sample mean and variance stabilize as number of Monte Carlo (NMC) realization increases. Figure 3 shows how the conditional sample mean $h^N(\mathbf{x})$ and variance $S_h^2(\mathbf{x})$ of head at grid point (4.0,2.0) vary with NMC at times $t = 1, 5, 20$. Although the conditional sample means $h^N(\mathbf{x})$ become stable after about 1000 realizations, the conditional sample variances $S_h^2(\mathbf{x})$ require at least 2000 realizations to exhibit partial stabilization. The stabilization of flux variance requires many additional realizations.

Figure 4a compares contours of conditional mean head at time $t = 5$ as computed using moment (dashed) and Monte Carlo (solid) results. Figure 4b illustrates how conditional mean head at point $(4.0, 2.0)$ evolves with time. Analogous depictions of conditional head variance are presented in Figure 5. In both cases the moment and Monte Carlo solutions compare very well. Uncertainty is seen to decreases monotonically with time upstream and increase downstream of the point source. Readers interested in additional details concerning the space-time evolution of

the first two conditional moments of head and flux under these and similar conditions may want to consult [8].

8. COMPUTATIONAL EFFICIENCY

We compare our parallel moment and Monte Carlo algorithms in terms of their speedups and efficiencies. According to [15], speedup and efficiency are defined respectively as $S(p) = T(1)/T(p)$ and $E(p) = S(p)/p$, where $T(1)$ and $T(p)$ are runtimes of a serial code and a parallel code with p processors. Runtimes are measured when the codes run as batch jobs in a dedicated queue. When runtime varies from processor to processor, $T(p)$ is taken to be the longest among these runtimes.

Runtimes, speedups and efficiencies of our parallel moment and Monte Carlo codes using 1, 4 and 8 processors are listed for several variables in Table I. The performance of the codes is seen to be satisfactory on 4 processors but less so on 8 processors. This is due to an increase in overhead such as idling and communication between processors. Performance for second-order residual flux is the worst because the problem size is small (runtime using one processor is less than 3 minutes). As the number of processors increases, the size of each sub problem for local calculation decrease further, bringing about a relative increase in overhead. This causes efficiency to diminish. In our case, the master-slave style I/O operation does not affect performance. For example, the most output demanding calculation of zero-order mean Green's functions (requiring the generation of 39312 files) on 4 processors is done with more than 90% efficiency. The reason is that the output data set (13784 bytes for each file) is small compared to the bandwidth of 150 $Mbytes/\sec$. The efficiency of the parallel Monte Carlo code is lower than the average efficiency of parallel moment algorithm codes. It is possible that the former does not synchronize as well as the latter.

Table II compares moment and Monte Carlo runtimes required to compute the mean and variance of head using 1, 4 and 8 processors. Although zero- and second-order mean head are computed with serial codes, since corresponding runtimes are very short (less than 1 minute), comparison of MC and ME runtimes is still meaningful. Our moment algorithm clearly outperforms the Monte Carlo algorithm regardless of whether one uses one or multiple processors. For example, the time required to compute mean head using the moment algorithm on one processor is about one fourth the corresponding time required for Monte Carlo simulations; the time required to compute head variance using the moment algorithm is about one half of the corresponding Monte Carlo runtime. The ratio between moment and Monte Carlo runtimes decreases further as the number of processors increases.

To explore the effect of grid size on parallel performance of our moment algorithm we reduce the number of elements, M, from 800 to 600 and 400. Figures 6a-c show how efficiency varies with M for three different moments. Cleary, performance improves with grid size. Figure 6d indicates that the opposite is true for Monte Carlo simulations. Hence the computational advantage of our moment algorithm over Monte Carlo simulations improves with grid size.

9. SUMMARY

We proposed an efficient parallel computational algorithm for leading conditional moments of transient flow variables in randomly heterogeneous porous media. Our algorithm is considerably faster than Monte Carlo simulations and its relative computational efficiency improves further with grid size. The algorithm is based on Green's functions which, once computed for a given configuration of boundary conditions, can be used repeatedly to investigate

the effect of various boundary and source scenarios on mean flow behavior and the corresponding uncertainty.

10. ACKNOWLEDGEMENT

This research was supported by the U.S. Nuclear Regulatory Commission under contract NRC-04-95-038, and by NSF/ITR Grant EAR-0110289.

Appendix A

We approximate $< \overline{h}^{(0)}(\mathbf{x},\lambda) >_c$ and $< \overline{h}^{(2)}(\mathbf{x},\lambda) >_c$ as

$$< \overline{h}^{(0)}(\mathbf{x},\lambda) >_c \approx \sum_{m=1}^{N} \overline{h}_m^{(0)}(\lambda)\varphi_m(\mathbf{x}) \qquad < \overline{h}^{(2)}(\mathbf{x},\lambda) >_c \approx \sum_{m=1}^{N} \overline{h}_m^{(2)}(\lambda)\varphi_m(\mathbf{x}) \tag{A1}$$

Substituting (17) into (18), multiplying by the basis function, integrating over Ω and applying Green's first identity leads to

$$\begin{aligned} &\int_\Omega K_G(\mathbf{x})\nabla < \overline{h}^{(2)}(\mathbf{x},\lambda) >_c \cdot\nabla\varphi_n(\mathbf{x})d\mathbf{x} + \int_\Omega K_G(\mathbf{x})\frac{\sigma_Y^2(\mathbf{x})}{\mathbf{2}}\nabla < \overline{h}^{(0)}(\mathbf{x},\lambda) >_c \cdot\nabla\varphi_n(\mathbf{x})d\mathbf{x} \\ &-\int_\Omega \overline{\mathbf{r}}_c^{(2)}(\mathbf{x},\lambda)\cdot\nabla\varphi_n(\mathbf{x})d\mathbf{x} + \int_\Omega S_s(\mathbf{x})\lambda < \overline{h}^{(2)}(\mathbf{x},\lambda) >_c \varphi_n(\mathbf{x})d\mathbf{x} = \\ &\int_{\Gamma_D} \varphi_n(\mathbf{x})[K_G(\mathbf{x})\nabla < \overline{h}^{(2)}(\mathbf{x},\lambda) >_c + K_G(\mathbf{x})\frac{\sigma_Y^2(\mathbf{x})}{2}\nabla < \overline{h}^{(0)}(\mathbf{x},\lambda) >_c - \overline{\mathbf{r}}_c^{(2)}(\mathbf{x},\lambda)]\cdot\mathbf{n}(\mathbf{x})d\mathbf{x} \end{aligned} \tag{A2}$$

where the boundary integral vanishes on the Neuman boundary Γ_N by virtue of (20). Recalling that $-< \overline{Q}(\mathbf{x},\lambda) >= K_G(\mathbf{x})\nabla < \overline{h}^{(0)}(\mathbf{x},\lambda) >_c \cdot\mathbf{n}(\mathbf{x})$ (16) and $< \overline{h}^{(2)}(\mathbf{x},\lambda) >_c$ is zero on the Dirichlet boundary, the right hand side of (A2) becomes

$$-\int_{\Gamma_D} \frac{\sigma_Y^2(\mathbf{x})}{2} < \overline{Q}(\mathbf{x},\lambda) > \varphi_n(\mathbf{x})d\mathbf{x} - \int_{\Gamma_D} \overline{\mathbf{r}}_c^{(2)}(\mathbf{x},\lambda)\cdot\mathbf{n}(\mathbf{x})\varphi_n(\mathbf{x})d\mathbf{x} \tag{A3}$$

Substituting (A1) and (A3) into (A2) leads directly to equations (30) – (35).

Appendix B

In a two-dimensional domain $< \overline{G}^{(0)}(\mathbf{y},\mathbf{x},\lambda) >_c$ is a four-dimensional function. We approximate it as the weighted sum of its values at all *N* nodes in the **x**- and **y**-plane according to

$$< \bar{G}^{(0)}(\mathbf{y},\mathbf{x},\lambda) >_c \approx \sum_{i=1}^{N_x}\sum_{j=1}^{N_y} \bar{G}_{ij}^{(0)}(\lambda)\varphi_i(\mathbf{x})\varphi_j(\mathbf{y}) \tag{B1}$$

where $\bar{G}_{ij}^{(0)}(\lambda)$ is the zero-order conditional mean Green's function in the Laplace domain at node i in the **x**-plane due to a source of unit strength at node j in the **y**-plane. Clearly $\bar{G}_{ij}^{(0)}(\lambda) \equiv \bar{G}_{ji}^{(0)}(\lambda)$.

Substituting the nodal approximation of zero-order mean hydraulic head (A1) and Green's function (B1) into (21) leads to

$$\bar{\mathbf{r}}_c^{(2)}(\mathbf{x},\lambda) = \int_\Omega K_G(\mathbf{x})K_G(\mathbf{y}) < Y'(\mathbf{x})Y'(\mathbf{y}) >_c \sum_{i=1}^{N}\sum_{j=1}^{N} \bar{G}_{ij}^{(0)}(\lambda)\nabla_{\mathbf{x}}\varphi_i(\mathbf{x})\nabla_{\mathbf{y}}^T\varphi_j(\mathbf{y})\sum_{k=1}^{N_y}\bar{h}_k^{(0)}(\lambda)\nabla_{\mathbf{y}}\varphi_k(\mathbf{y})d\mathbf{y} \tag{B2}$$

Approximating the domain integral in the **y**-plane by a summation of integrals over elements in the **y**-plane gives

$$\bar{\mathbf{r}}_c^{(2)}(\mathbf{x},\lambda) = \sum_{i=1}^{N} K_G(\mathbf{x})\nabla_{\mathbf{x}}\varphi_i(\mathbf{x})\sum_{e'=1}^{M_y} K_G(\mathbf{y}) < Y'(\mathbf{x})Y'(\mathbf{y}) >_c \sum_{j=1}^{N_y}\sum_{k=1}^{N_y} \bar{G}_{ij}^{(0)ee'}(\lambda)\bar{h}_k^{(0)e'}(\lambda)\Delta_{jk}^{e'e'} \tag{B3}$$

where N_y is the number of nodes in element e' within the **y**-plane; M_y is the number of elements in the **y**-plane; $\bar{h}_k^{(0)e'}(\lambda)$ is $\bar{h}^{(0)}(\mathbf{y},\lambda)$ at node k of element e' in the **y**-plane; and $\Delta_{ij}^{e'e'}$ is given by (37). Treating log hydraulic conductivity as a constant in each element, the covariance $< Y'(\mathbf{x})Y'(\mathbf{y}) >_c$ between any points **x** in element e and **y** in element e' is approximated by $< Y'(\mathbf{x}^e)Y'(\mathbf{y}^{e'}) >_c$, where $\mathbf{x}^e$ is the centroid of element e and $\mathbf{y}^{e'}$ is the centroid of element e'. Evaluating the second-order residual flux at each element center $\mathbf{x}^e$ by means of (B3) yields (36). Equations (40) – (42) are obtained in a similar manner.

REFERENCES

1. G. Dagan and S. P. Neuman (Editors), *Subsurface Flow and Transport, A stochastic Approach*, International Hydrology Series, Cambridge University Press, Cambridge U. K., (1997).
2. Kitanidis, P. K., *Introduction to Geostatistics*, Cambridge University Press, Cambridge U. K., (1997).
3. Zhang, D., *Stochastic Methods for Flow in Porous Media*, Academic Press, (2001).
4. D. M. Tartakovsky, and S. P. Neuman, Transient flow in bounded randomly heterogeneous domains 1. Exact conditional moment equations and recursive approximations, *Water Resour. Res.* **34**, 1 (1998).
5. A. Guadagnini and S. P. Neuman, Nonlocal and localized analyses of conditional mean steady state flow in bounded randomly nonuniform domains 1. Theory and computational approach, *Water Resour. Res.* **35**, 2999 (1999).
6. A. Guadagnini, and S. P. Neuman, Nonlocal and localized analyses of conditional mean steady state flow in bounded randomly nonuniform domains 2. Computational Examples. *Water Resour. Res.* **35**, 3019 (1999).
7. F. R. De Hoog, J. H. Knight, and A. N. Stokes, An improved method for numerical inversion of Laplace transform, *SIAM J. Sci. Stat. Comput.* **3**, 357 (1982).
8. M. Ye, Parallel finite element Laplace transform algorithm for transient flow in bounded randomly heterogeneous domains, Ph.D. dissertation, Univ. of Arizona, Tucson, 2002.
9. K. S. Crump, Numerical inverse of Laplace transform using a Fourier series approximation, *J. Assoc. Comput. Mach.* **23**, 89 (1976).
10. Message Passing Interface Forum, available at www-unix.mcs.anl.gov/mpi/.

11. IMSL software package, available at *www.vni.com/products/imsl/*.
12. K. A. Cliffe, I. G. Graham, R. Scheichl, and L. Stals, Parallel computation of flow in heterogeneous media modeled by mixed finite elements, *J. Comput. Phy.* **164**, 258 (2000).
13. G. Pini, and M. Putti, Parallel finite element Laplace transform method for the non-equilibrium groundwater transport equation, *Int. J. Numer. Methods Eng.* **40**, 2653 (1997).
14. C. V. Deutsch and A. G. Journel, *GSLIB: Geostatistical Software Library and User's Guide (second edition)* Oxford University Press, New York, (1998).
15. P. Pacheco, *Parallel Computing with MPI*, Morgan Kaufmann Publishers, San Francisco, (1997).

LIST OF FIGURES

FIG. 1. Computational grid, conditioning points (black squares), boundary conditions and point source (black circle).

FIG. 2. (a) Image of conditional sample variance $S_Y^2(\mathbf{x})$ and its profiles along sections (b) $x_2 = 2.5$ and (c) $x_2 = 1.9$ obtained from 2000 conditional Monte Carlo realizations with unconditional variance $\sigma_Y^2 = 1$ and integral scale $l = 1$.

FIG. 3. Sample mean (a) and variance (b) of head at $x_1 = 4, x_2 = 2$ versus NMC for $\sigma_Y^2 = 1, l = 1$.

FIG. 4. (a) Contours of conditional mean head at time $t = 5$ and (b) conditional mean head versus time at point $(4.0, 2.0)$ obtained using moment (dashed) and Monte Carlo (solid) algorithms for $\sigma_Y^2 = 1, l = 1$.

FIG. 5. (a) Contours of conditional head variance at time $t = 5$ and (b) conditional head variance versus time at points B $(2.0, 2.0)$ and C $(6.0, 2.0)$ obtained using moment (dashed) and Monte Carlo (solid) algorithms for $\sigma_Y^2 = 1, l = 1$.

FIG. 6. Effect of number of elements *M* on efficiency in computing (a) zero-order mean Green's function $< \overline{G}^{(0)} >_c$, (b) second-order cross-covariance $\overline{u}_c^{(2)}$, (c) second-order head variance $\overline{C}_{hc}^{(2)}$ using moment and (d) Monte Carlo algorithms for $\sigma_Y^2 = 1, l = 1$.

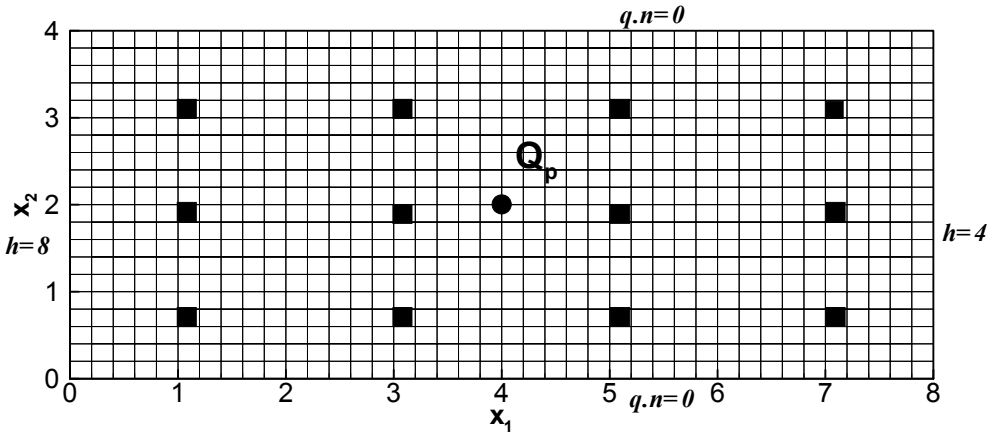

FIG. 1

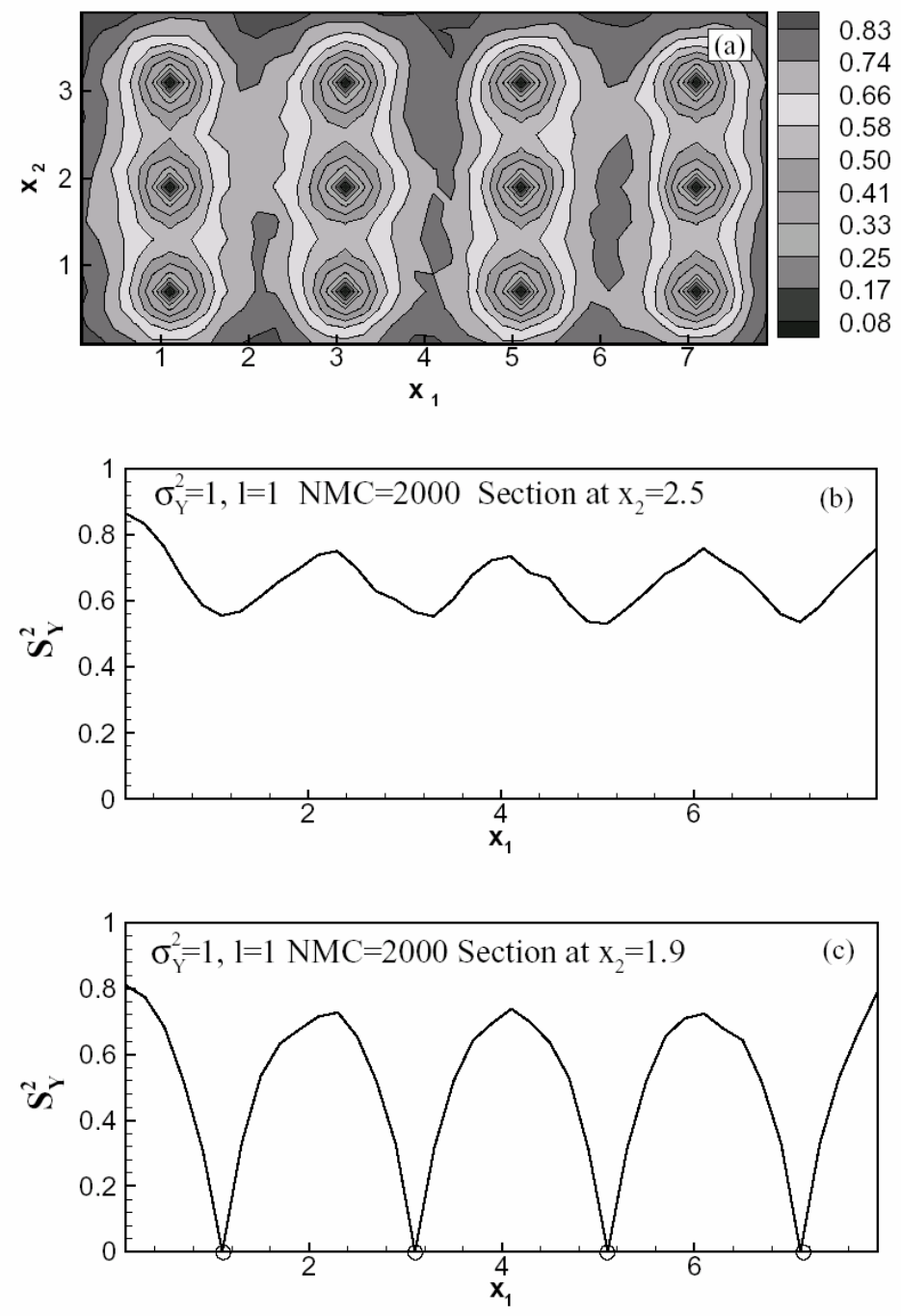
(a)
0.83
0.74
0.66
0.58
0.50
0.41
0.33
0.25
0.17
0.08
x 2
x 1
σ²Y=1, l=1 NMC=2000 Section at x2=2.5
(b)
S²Y
x1
σ²Y=1, l=1 NMC=2000 Section at x2=1.9
(c)
S²Y
x1

FIG. 2

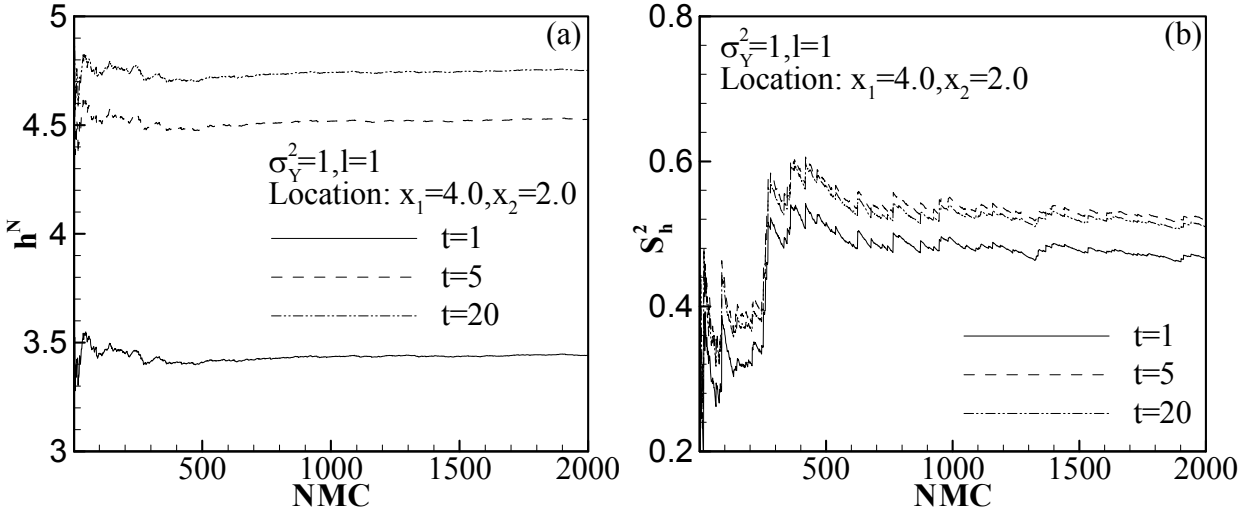
(a)
σ_Y^2=1,l=1
Location: x_1=4.0,x_2=2.0
t=1
t=5
t=20
$\bar{h}^N$
NMC
(b)
σ_Y^2=1,l=1
Location: x_1=4.0,x_2=2.0
t=1
t=5
t=20
S_h^2
NMC

FIG. 3

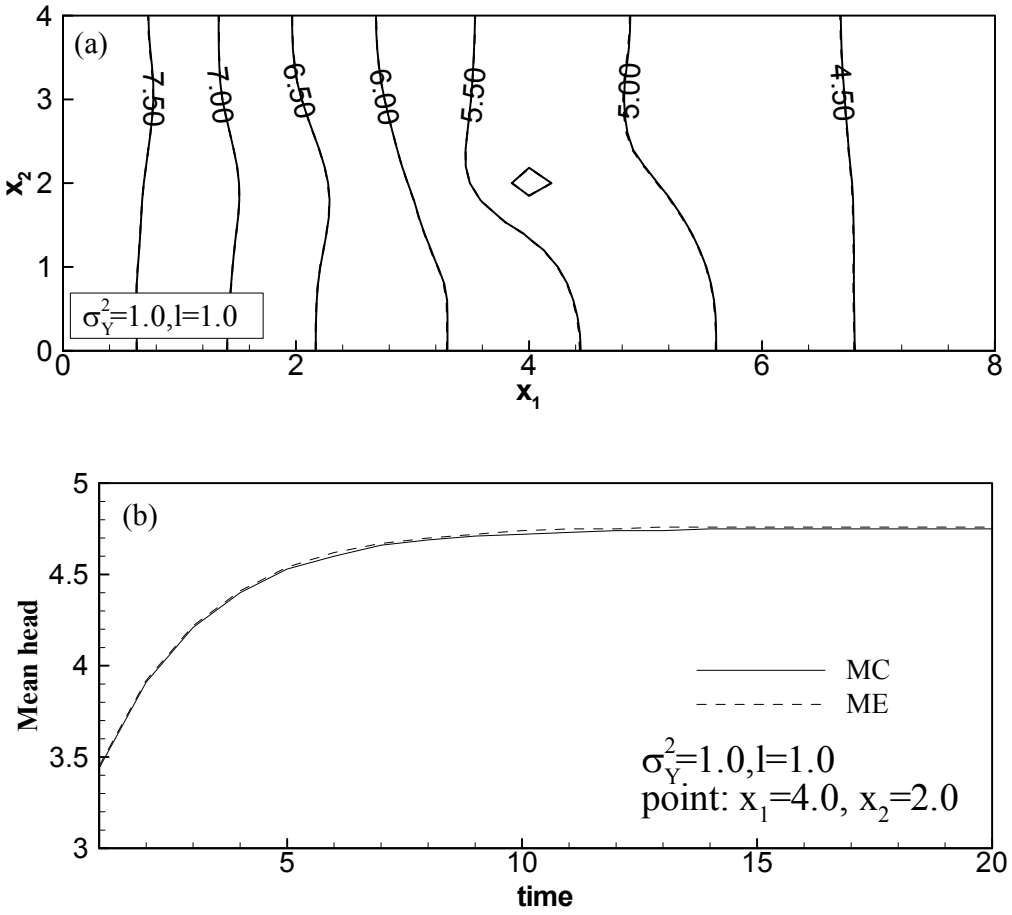
(a)
7.50
7.00
6.50
6.00
5.50
5.00
4.50
σ_Y^2=1.0,l=1.0
x_2
x_1
(b)
Mean head
time
MC
ME
σ_Y^2=1.0,l=1.0
point: x_1=4.0, x_2=2.0

FIG. 4

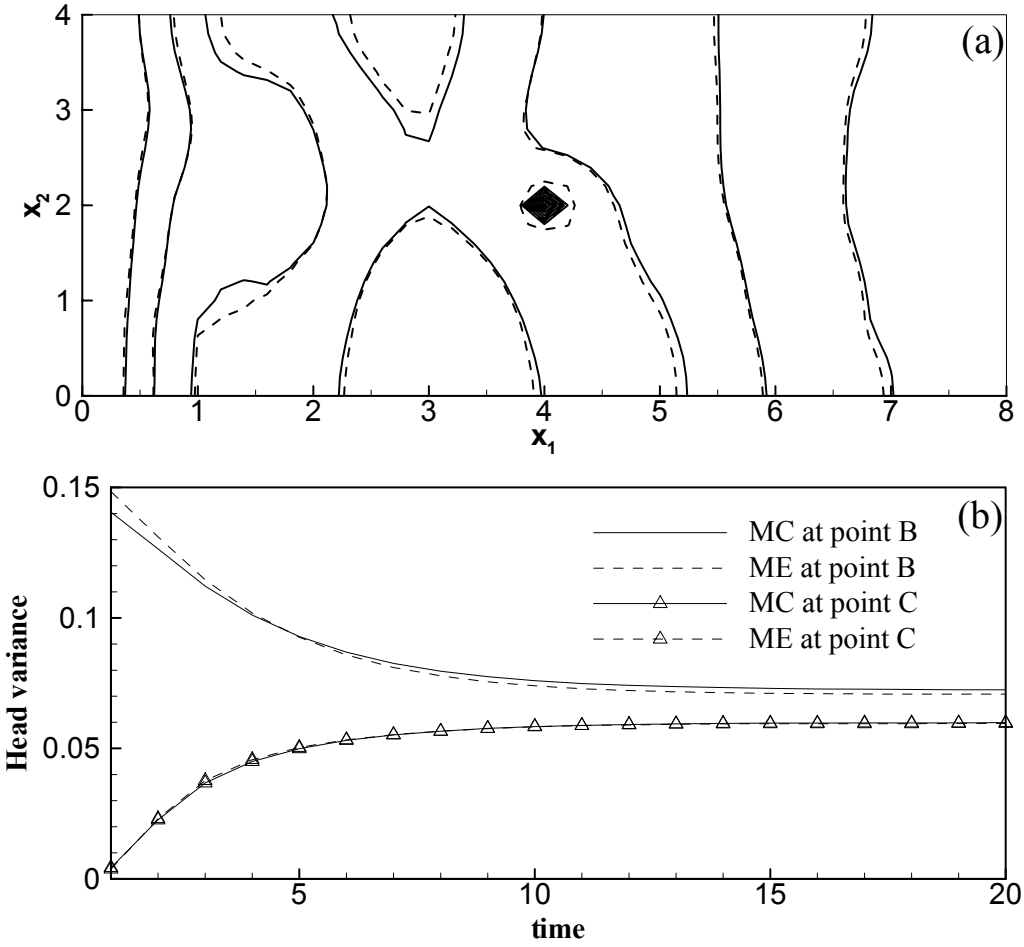
(a)
x_2
x_1
0
1
2
3
4
5
6
7
8
(b)
Head variance
time
0.15
0.1
0.05
0
5
10
15
20
MC at point B
ME at point B
MC at point C
ME at point C

FIG. 5

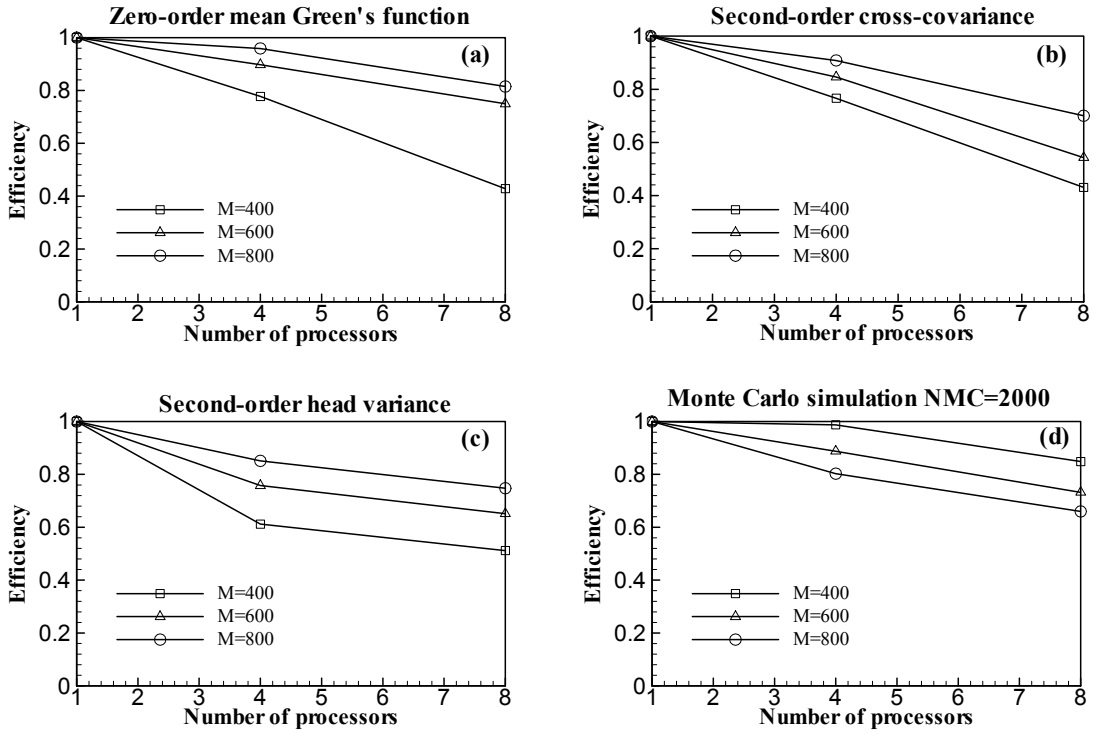
Zero-order mean Green's function
(a)
Second-order cross-covariance
(b)
Second-order head variance
(c)
Monte Carlo simulation NMC=2000
(d)
Efficiency
Number of processors
M=400
M=600
M=800

FIG. 6

LIST OF TABLES

Table I

	Monte Carlo	Moment algorithm			
Variables	2000 Realizations	$< \overline{G}^{(0)} >_c$	$\overline{\mathbf{r}}_c^{(2)}$	$\overline{u}_c^{(2)}$	$\overline{C}_{hc}^{(2)}$
$T(1)$ (sec)	49900.65	12523.17	171.00	11235.32	5854.05
$T(4)$ (sec)	15537.42	3265.90	54.71	3091.83	1719.27
$S(4)$	3.21	3.84	3.13	3.63	3.40
$E(4)$ (%)	80.29	95.89	78.14	90.85	85.12
$T(8)$ (sec)	9454.74	1920.97	37.37	2005.68	863.19
$S(8)$	5.28	6.52	4.58	5.60	6.78
$E(8)$ (%)	65.98	81.49	57.20	70.02	84.77

Table II

Runtime \ Variables		Mean Head	Head Variance
P=1	MC (min)	831.90	831.90
	ME (min)	212.83	494.30
P=4	MC (min)	259.20	259.20
	ME (min)	56.59	135.36
P=8	MC (min)	157.80	157.80
	ME (min)	33.90	80.59